The First Organically Templated Tetravalent Uranium Phosphates with Dimer-Structured Topologies

Yu-Lun Lai,[†] Ray-Kuang Chiang,[‡] Kwang-Hwa Lii,[§] and Sue-Lein Wang*[,†]

Department of Chemistry, National Tsing Hua University, Hsinchu 30013, Taiwan, Department of Electronic Materials, Far East University, Tainan 74448, Taiwan, and Department of Chemistry, National Central University, Chungli 32054, Taiwan

Received September 28, 2007. Revised Manuscript Received November 28, 2007

Four new organically templated uranium(IV) phosphates, $(C_4H_{16}N_3)[U_2F_3(PO_4)_2(HPO_4)]$ (**1**), $(C_6H_{21}N_4)[U_2F_4(PO_4)(HPO_4)_2]$ (**2**), $(C_4H_{16}N_3)_2[U_2F_{10}(HPO_4)_2]$ (**3**), and $(C_6H_{16}N_2)_2(UF_7)(H_2PO_4)$ (**4**), have been successfully synthesized in pure-phase form under mild solvothermal conditions and characterized by single-crystal X-ray diffraction, magnetic susceptibility, thermogravimetric analysis (TGA), elemental analysis, inductively coupled plasma−atomic emission spectroscopy, and fluorine analysis. They are the first tetravalent uranium phosphates with encapsulated organic templates ever reported. All four materials display unique dimer-structured topologies with various dimensionalities in the inorganic/hydrogen-bonded networks. In this series, U^{4+} ions are located in the center of bicapped trigonal prisms of UFO_7, UF_2O_6, UF_6O_2, or UF_8, from which edge-sharing $U_2F_mO_{14-m}$ dimers ($m = 2$ and 4 in **1**, $m = 4$ in **2**, $m = 10$ in **3**, and $m = 14$ in **4**) are formed. The less-fluorinated $U_2F_2O_{12}$ and $U_2F_4O_{10}$ dimers are connected to eight and six phosphate groups to give two-dimensional layer and one-dimensional chain structures, respectively; the more-fluorinated $U_2F_{10}O_4$ and fully fluorinated U_2F_{14} dimers are respectively attached by two or zero phosphate groups to form clustered structures. TGA results indicated that the layered structure of **1** could sustain heating up to ~300 °C and the thermal stability of the series steadily decreased with decreasing structural dimensionality. The 4+ oxidation state of uranium was confirmed by bond-valence-sum calculations and magnetic susceptibility measurements. In view of radioactive mobility, we discovered that **1** and **2** could be more stable than UO_2 under sufficiently oxidizing conditions. Crystal data: triclinic, space group $P\bar{1}$, $a = 9.1657(4)$ Å, $b = 10.0618(4)$ Å, $c = 10.7584(4)$ Å, $\alpha = 73.668(1)°$, $\beta = 65.366(1)°$, $\gamma = 65.916(1)°$, and $Z = 2$ for **1**; monoclinic, $P2_1/c$, $a = 11.1124(4)$ Å, $b = 19.6830(8)$ Å, $c = 10.1466(4)$ Å, $\beta = 114.362(1)°$, and $Z = 4$ for **2**; monoclinic, space group $P2_1/n$, $a = 18.383(1)$ Å, $b = 7.8448(6)$ Å, $c = 18.442(1)$ Å, $\beta = 113.967(1)°$, and $Z = 4$ for **3**; monoclinic, $P2_1/c$, $a = 10.2346(9)$ Å, $b = 23.846(2)$ Å, $c = 8.8091(8)$ Å, $\beta = 93.459(2)°$, and $Z = 4$ for **4**.

Introduction

In the past decade, the chemistry of actinides such as uranium has attracted considerable attention because of its relevance to the geological repository for nuclear wastes[1,2] as well as to the catalytic properties,[3] ionic conductivities,[4] and remarkable structural versatilities of these species.[5–14] The structures of uranium phosphates are of particular interest since they are principal for understanding the mobility of uranium in the environment.[15] Uranium can exist in the 3+, 4+, 5+, and 6+ oxidation states, but only the 4+ and 6+ states are stable enough to be of practical importance. Uranium in these two oxidation states, however, shows different migration rates in a subsurface environment. It is noteworthy that reduced U^{4+} species are sparingly soluble and less mobile than U^{6+} species in soil.[16] In contrast to the abundance of hexavalent uranium compounds with assorted open-framework structures, only a limited number of tetravalent uranium phosphates, most with condensed structures, have been documented.[17] It would be interesting to exploit

* To whom correspondence should be addressed. Fax: 886-35-711082. E-mail: slwang@mx.nthu.edu.tw.
[†] National Tsing Hua University.
[‡] Far East University.
[§] National Central University.

(1) Jackson, J. M.; Burns, P. C. *Can. Mineral.* **2001**, *39*, 187.
(2) Burns, P. C.; Olson, R. A.; Finch, R. J.; Hanchar, J. M.; Thibault, Y. *J. Nucl. Mater.* **2000**, *278*, 290.
(3) Hutchings, G. J.; Heneghan, C. S.; Hudson, I. D.; Taylor, S. H. *Nature* **1996**, *384*, 341.
(4) Poojary, D. M.; Grohol, D.; Clearfield, A. *Angew. Chem., Int. Ed.* **1995**, *34*, 1508.
(5) Altrecht-Schmitt, T. E. *Angew. Chem., Int. Ed.* **2005**, *44*, 4836.
(6) Kahlenberg, V.; Tananaev, I. G.; Kaindl, R.; Mersdorf, E.; Myasoedov, B. F. *J. Am. Chem. Soc.* **2005**, *127*, 1072.
(7) Chen, C. S.; Lee, S. F.; Lii, K. H. *J. Am. Chem. Soc.* **2005**, *127*, 12208.
(8) Krivovichev, S. V.; Armbruster, T.; Chernyshov, D. Y.; Burns, P. C.; Nazarchuk, E. V.; Depmeier, W. *Microporous Mesoporous Mater.* **2005**, *78*, 225.
(9) Francis, R. J.; Halasyamani, P. S.; O'Hare, D. *Angew. Chem., Int. Ed.* **1998**, *37*, 2214.
(10) Wang, C. M.; Liao, C. H.; Lin, H. M.; Lii, K. H. *Inorg. Chem.* **2004**, *43*, 8239.
(11) Wang, X.; Huang, J.; Jacobson, A. J. *J. Am. Chem. Soc.* **2002**, *124*, 15190.
(12) Francis, R. J.; Halasyamani, P. S.; Bee, J. S.; O'Hare, D. *J. Am. Chem. Soc.* **1999**, *121*, 1609.
(13) Walker, S. M.; Halasyamani, P. S.; Allen, S.; O'Hare, D. *J. Am. Chem. Soc.* **1999**, *121*, 10513.
(14) Ok, K. M.; Michael, B. D.; O'Hare, D. *J. Mater. Chem.* **2006**, *16*, 3366.
(15) Silva, R. J.; Nitsche, H. *Radiochim. Acta* **1995**, *70−71*, 377.
(16) Zhou, P.; Gu, B. H. *Environ. Sci. Technol.* **2005**, *39*, 4435.
(17) Brandel, V.; Dacheux, N. *J. Solid State Chem.* **2004**, *177*, 4743 and references cited therein.

10.1021/cm7027959 CCC: $40.75
Published on Web 01/01/2008

the synthesis of uranium(IV) phosphates with more diversified structures and find new physicochemical properties to meet the demands of current and next-generation technologies.

In recent years, the strategy of using organic templates as structure-directing reagents in the formation of microporous transition-metal phosphates has been successfully extended to the synthesis of open-framework uranium phosphates.[18–20] However, the phosphates synthesized in this way include only hexavalent uranium phases. Successful synthesis of organically templated tetravalent uranium phosphates has not been reported to date. It is unclear how the formation of new phosphate matrixes that contain U^{4+} centers could be directed effectively by organic templates. We have noted that previously reported uranium phosphates were all synthesized using water as the sole solvent. However, organic solvents have already played an important role in the crystallization of many organic-templated structures.[21–24] Such a vantage has not yet been observed and synchronously exercised in uranium chemistry. In this study, we have commenced using organic solvents in combination with variously shaped polyamine templates in the synthesis of uranium phosphates. Successful matches within the template−solvent system have allowed us to prepare the first four examples of organically templated tetravalent uranium phosphates: $(C_4H_{16}N_3)[U_2F_3(PO_4)_2(HPO_4)]$ (**1**), $(C_6H_{21}N_4)[U_2F_4(PO_4)(HPO_4)_2]$ (**2**), $(C_4H_{16}N_3)_2[U_2F_{10}(HPO_4)_2]$ (**3**), and $(C_6H_{16}N_2)_2(UF_7)(H_2PO_4)$ (**4**). They exhibit four unique dimer-structured topologies with various dimensionalities and interesting hydrogen-bonding networks. The results from oxidizing experiments under ambient conditions combined with magnetic studies indicated that the higher-dimensional structures of **1** and **2** were more stable and could be less mobile in the environment than uraninite.[25] Here we report the syntheses, crystal structures, and magnetic and thermal properties of the first organically templated uranium(IV) phosphates. We also discuss factors controlling the formation of various dimer motifs in these structures, organic template−solvent effects, and structure-related properties.

Experimental Section

Caution: Although all uranium materials used in this study were depleted, extra care and good laboratory practice should always be used when handling these uranium compounds.

Synthesis and Initial Characterization. Chemicals of reagent grade were used as received. Solvothermal reactions were carried out at 160 °C for 3 days in Teflon-lined acid digestion autoclaves (23 mL internal volume), and then the reaction mixtures were slowly cooled to room temperature at a rate of 6 °C h^{-1}. The depleted uranyl acetate dihydrate, $UO_2Ac_2 \cdot 2H_2O$ (Ac = CH_3CO_2), was used as the single source of U. In this work, all reaction mixtures contained exactly the same amounts of $UO_2Ac_2 \cdot 2H_2O$, H_3PO_4, HF, and organic amine template in the molar ratio 1:24:18:16 but had different solvents. We noted that the organic solvent system was crucial in preparing different tetravalent uranium phosphate phases. Light-green, needle-shaped crystals of $(H_3dien)[U_2F_3(PO_4)_2(HPO_4)]$ (**1**, dien = diethylenetriamine, $C_4H_{13}N_3$) were obtained from the reaction mixture as a single-phase product (~83% yield based on U content) using dien as the template and 50% 1-butanol (Bt) solution as the solvent. Changing the template to tren [tris(2-aminoethyl)amine, $C_6H_{18}N_4$] and the organic part of the solvent to ethylene glycol (EG) yielded a single-phase product of light-green, threadlike crystals of $(H_3tren)[U_2F_4(PO_4)(HPO_4)_2]$ (**2**) (~80% yield). When the template was changed back to dien in the same EG/H_2O solvent, a few green plates of $(H_3dien)_2[U_2F_{10}(HPO_4)_2]$ (**3**) were observed to emerge in the product. To attain a single-phase product of **3**, it was necessary to replace the mixed EG/H_2O solvent by pure EG. At this stage, we perceived from the results of single-crystal analysis (see below) that the organic solvent could have an adverse effect on the association between phosphates and U^{4+} ions. This conjecture led us to further explore reactions involving the use of solely organic solvents. However, attempting to manipulate the number of phosphate tetrahedra on uranium always failed with the use of triamines. In the end, only the combination of the diamine template dach (diaminocyclohexane, $C_6H_{14}N_2$) with the mixed organic solvent Bt/EG (designated as the dach−Bt/EG system) could produce a single-phase product of light-green, thin-bladed crystals of $(H_2dach)_2(UF_7)(H_2PO_4)$ (**4**). A diagram showing the solvent systems and the products obtained therein is provided in Figure 1. In this study, all measurements (see below) were performed on samples whose individual purities were preliminarily checked using powder X-ray diffraction (XRD) patterns. The oxidation state of uranium was verified by bond-valence-sum calculations[26] and the F content in each compound by fluorine analysis. Inductively coupled plasma−atomic emission spectroscopy (ICP−AES) and elemental analysis (EA) confirmed the inorganic (U and P) and organic (C, H, N) components, respectively. The resistance of each compound against oxidation to U^{6+} was diagnosed by means of reactions with a 35% H_2O_2 solution under ambient conditions.

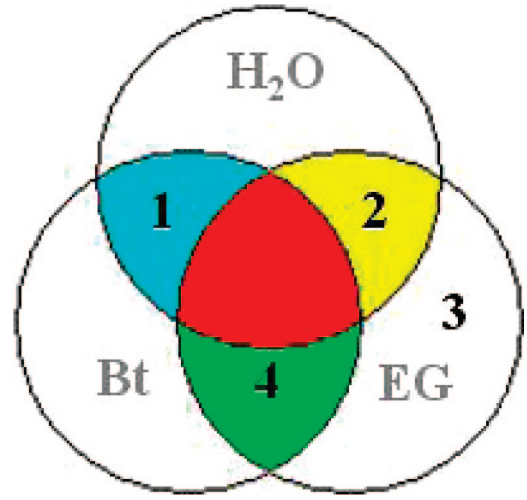

Figure 1. Schematic diagram showing the solvent systems and the individual compounds **1**–**4** prepared in pure phase form therein. Compounds **1**, **2**, and **4** were all synthesized in solvents mixed in a 1:1 ratio.

(18) Doran, M. B.; Stuart, C. L.; Norquist, A. J.; O'Hare, D. *Chem. Mater.* **2004**, *16*, 565.
(19) Danis, J. A.; Runde, W. H.; Scott, B.; Fettinger, J.; Eichhorn, B. *Chem. Commun.* **2001**, 2378.
(20) Locock, A. J.; Burns, P. C. *J. Solid State Chem.* **2004**, *177*, 2675.
(21) Morris, R.; Weigel, S. L. *Chem. Soc. Rev.* **1997**, *26*, 309.
(22) Lai, Y. L.; Lii, K. H.; Wang, S. L. *J. Am. Chem. Soc.* **2007**, *129*, 5350.
(23) Liao, Y. C.; Lin, C. H.; Wang, S. L. *J. Am. Chem. Soc.* **2005**, *127*, 9986.
(24) Medina, M. E.; Iglesias, M.; Gutiérrez-Puebla, E.; Monge, M. A. *J. Mater. Chem.* **2004**, *14*, 845.
(25) Frazier, S. W.; Kretzschmar, R.; Kraemer, S. M. *Environ. Sci. Technol.* **2005**, *39*, 5709.
(26) Brese, N. E.; O'Keeffe, M. *Acta Crystallogr.* **1991**, *B47*, 192.

Table 1. Crystallographic Data for $(C_4H_{16}N_3)[U_2F_3(PO_4)_2(HPO_4)]$ (1), $(C_6H_{21}N_4)[U_2F_4(PO_4)(HPO_4)_2]$ (2), $(C_4H_{16}N_3)_2[U_2F_{10}(HPO_4)_2]$ (3), and $(C_6H_{16}N_2)_2(UF_7)(H_2PO_4)$ (4)

	1	2	3	4
chemical formula	$C_4H_{17}N_3F_3O_{12}P_3U_2$	$C_6H_{23}N_4F_4O_{12}P_3U_2$	$C_8H_{34}N_6F_{10}O_8P_2U_2$	$C_{12}H_{34}N_4F_7O_4PU$
fw	925.18	988.25	1070.41	700.41
a (Å)	9.1657(4)	11.1124(4)	18.383(1)	10.2346(9)
b (Å)	10.0618(4)	19.6830(8)	7.8448(6)	23.846(2)
c (Å)	10.7584(4)	10.1466(4)	18.442(1)	8.8091(8)
α (deg)	73.668(1)	90.00	90.00	90.00
β (deg)	65.366(1)	104.019(1)	113.967(1)	93.459(2)
γ (deg)	65.916(1)	90.00	90.00	90.00
V (Å^3)	815.95(6)	2021.7(1)	2430.2(3)	2146.0(3)
Z	2	4	4	4
space group	$P\bar{1}$ (No. 2)	$P2_1/c$ (No. 14)	$P2_1/n$ (No. 14)	$P2_1/c$ (No. 14)
T (°C)	20	20	20	20
λ(Mo Kα) (Å)	0.71073	0.71073	0.71073	0.71073
ρ_{calcd} (g cm^{-3})	3.766	3.247	2.926	2.131
μ(Mo Kα) (cm^{-1})	202.19	163.40	135.67	77.22
R_1[a]	0.0247	0.0271	0.0288	0.0382
wR_2[b]	0.0528	0.0606	0.0635	0.0917

[a] $R_1 = ||F_o| - |F_c||/|F_o|$ for $F_o > 4\sigma(F_o)$. [b] w$R_2 = 1/[\sigma^2(F_o^2) + (aP)^2 + bP]$, where $P = [\max(F_o)^2 + 2(F_c)^2]/3$ and a/b = 0.0240/0.00 for **1**, 0.0352/4.01 for **2**, 0.0332/0.00 for **3**, and 0.0765/0.00 for **4**.

Analysis of Single-Crystal Structure. Crystals of dimensions 0.05 × 0.05 × 0.20 mm for **1** and **2**, 0.05 × 0.05 × 0.10 mm for **3**, and 0.05 × 0.05 × 0.12 mm for **4** were selected for indexing and collection of intensity data at room temperature. Diffraction measurements were performed using a Bruker SMART APEX diffractometer system equipped with a normal-focus, 3 kW sealed-tube X-ray source (λ = 0.71073 Å). Intensity data were collected in 1271 (or 2070 for the triclinic cell) frames with increasing ω (0.3° per frame). Unit-cell dimensions were determined by least-squares fits of 4038 reflections for **1**, 5004 reflections for **2**, 4299 reflections for **3**, and 5175 reflections for **4**. Empirical absorption corrections based on symmetry equivalents were applied (T_{min}/T_{max} = 0.55/0.98 for **1**, 0.61/0.98 for **2**, 0.49/0.97 for **3**, and 0.48/0.93 for **4**). On the basis of systematic absences and intensity-distribution statistics, the space groups were determined to be $P\bar{1}$ for **1**, $P2_1/c$ for **2** and **4**, and $P2_1/n$ for **3**. All four structures were solved by direct methods, with nonhydrogen atoms located on electron-density maps. Bond-valence-sum calculations were used to assign the atoms O(1) in **1**, O(4) and O(12) in **2**, O(4) and O(7) in **3**, and O(1) and O(3) in **4** to hydroxyl groups. Most of the H atoms of the phosphate OH groups and the amine cations could be identified through careful scrutiny of final difference maps. The final cycles of refinement, including the atomic coordinates and anisotropic thermal parameters for all non-H atoms and fixed atomic coordinates and isotropic thermal parameters for H atoms, converged at R_1 (wR_2) = 0.0247 (0.0528) for **1**, 0.0271 (0.0606) for **2**, 0.0288 (0.0635) for **3**, and 0.0382 (0.0917) for **4**. Neutral-atom scattering factors were used, and corrections for anomalous dispersion and secondary extinction were applied. All calculations were performed using the PC version of the SHELXTL program package.[27] Crystallographic data are listed in Table 1 and selected bond distances in Table 2. ORTEP drawings with atomic labeling are given in the Supporting Information.

Magnetic Susceptibility Measurements. Variable-temperature magnetic susceptibility [$\chi(T)$] data were measured from 2 to 300 K in a magnetic field of 5 kG using a Quantum Design SQUID magnetometer on powder samples of **1** (20.1 mg), **2** (97.8 mg), **3** (25.0 mg), and **4** (29.0 mg). The data were corrected for the inherent diamagnetic contribution using the procedure of Selwood.[28] The observed effective moments (μ_{eff}) ranged from 3.59 to 3.17 μ_B per U^{4+} ion at 300 K.

Thermogravimetric Analysis and Oxidizing Experiments. Thermogravimetric analysis (TGA) was performed on powder samples using a PerkinElmer TGA-7 analyzer. The data were measured under flowing air from room temperature to 900 °C with a heating rate of 10 °C min^{-1}. Oxidizing experiments were performed by reacting specific amounts of **1**−**4** (each containing 0.0198 mmol of uranium) with 35% hydrogen peroxide (1 mL for each sample). Individual resistances against oxidation of the tetravalent uranium samples into hexavalent forms were monitored by recording the amounts of time needed for the color of the sample to change completely from green into yellow; the observed values were 76 h for **1**, 48 h for **2**, 1 h for **3**, and 0.5 h for **4**. For comparison purposes, the same experiment was performed on a sample of UO_2, and the time needed for sufficient oxidation was 7 h. The plenitude of oxidation was confirmed using follow-up magnetic susceptibility measurements, which showed distinct diamagnetism for all of the oxidized samples.

Results and Discussion

Structure Description. Compounds **1**–**4** exclusively contain eight-coordinate U^{4+} ions with F^- and/or O_p (phosphate oxygen) ligands in a bicapped trigonal prismatic (BTP) geometry. Figure 2 depicts four kinds of observed BTP monomers, all of which exist in forms that have edge-sharing dimers as a common structural feature. Another common feature is the infinite chains that are built up from the dimers and phosphate tetrahedra; they are covalently bonded chains in **1** and **2** and hydrogen-bonded supramolecular chains in **3** and **4** (Figure 3). In each of the structures, the polyamine templates are fully protonated and associate with the inorganic part mainly by cation–anion charge interactions. Although all four structures show interesting hydrogen-bonded inorganic networks (Figure 4), we observed no significant hydrogen bonds between the amine templates and the inorganic part.

The structure of **1** is two-dimensional (2D) and contains $[UFO_5]_2O_2$ and $[UF_2O_4]_2O_2$ dimers respectively formed of UFO_7 and UF_2O_6 monomers sharing an O−O edge (2.660–2.753 Å). As shown in Figure 2, the $[UFO_5]_2O_2$ dimers are each attached by eight phosphate tetrahedra (six PO_4 and two HPO_4) to form the dimer motifs I, which can interlink with each other via corner-shared $P(2)O_4$ tetrahedra to produce the infinite

(27) Sheldrick, G. M. *SHELXTL Programs*, version 5.1; Bruker AXS GmbH: Karlsruhe, Germany, 1998.
(28) Selwood, P. W. *Magnetochemistry*; Interscience: New York, 1956.

Table 2. Selected Bond Lengths (Å) and Bond Valence Sums (Σs) for 1–4

		1			
U(1)−F(1)	2.190(3)	U(2)−F(2)	2.241(3)		
U(1)−O(5)[a]	2.230(4)	U(2)−F(3)	2.242(3)		
U(1)−O(6)	2.350(3)	U(2)−O(8)[c]	2.292(3)		
U(1)−O(4)	2.351(4)	U(2)−O(2)	2.296(4)		
U(1)−O(3)[b]	2.357(3)	U(2)−O(7)[d]	2.378(3)		
U(1)−O(9)[b]	2.395(3)	U(2)−O(10)	2.425(3)		
U(1)−O(11)	2.410(4)	U(2)−O(12)[e]	2.426(4)		
Σs[U(1)−O(F)] = 4.14		Σs[U(2)−O(F)] = 4.14			
P(1)−O(3)	1.512(4)	P(2)−O(8)	1.530(4)	P(3)−O(9)	1.521(4)
P(1)−O(2)	1.527(4)	P(2)−O(6)	1.536(4)	P(3)−O(10)	1.533(4)
P(1)−O(4)	1.535(4)	P(2)−O(7)	1.541(4)	P(3)−O(12)	1.544(4)
P(1)−O(1)	1.592(4)	P(2)−O(5)	1.543(4)	P(3)−O(11)	1.546(4)
Σs[P(1)−O] = 4.92		Σs[P(2)−O] = 4.96		Σs[P(3)−O] = 4.98	
		2			
U(1)−F(1)	2.214(3)	U(2)−F(4)	2.213(3)		
U(1)−O(1)[f]	2.267(4)	U(2)−O(10)[f]	2.248(4)		
U(1)−F(2)	2.274(3)	U(2)−F(3)	2.281(3)		
U(1)−O(11)	2.298(4)	U(2)−O(3)	2.329(4)		
U(1)−O(7)	2.381(4)	U(2)−O(8)	2.370(4)		
U(1)−O(9)[g]	2.411(4)	U(2)−O(2)[f]	2.379(4)		
U(1)−O(5)[g]	2.439(4)	U(2)−O(6)[f]	2.409(4)		
U(1)−O(7)[g]	2.542(4)	U(2)−O(6)	2.594(4)		
Σs[U(1)−O(F)] = 4.08		Σs[U(2)−O(F)] = 4.09			
P(1)−O(2)	1.519(4)	P(2)−O(8)	1.529(4)	P(3)−O(9)	1.515(4)
P(1)−O(1)	1.519(4)	P(2)−O(7)	1.533(4)	P(3)−O(11)	1.518(4)
P(1)−O(3)	1.520(4)	P(2)−O(6)	1.536(4)	P(3)−O(10)	1.524(4)
P(1)−O(4)	1.578(4)	P(2)−O(5)	1.540(4)	P(3)−O(12)	1.576(4)
Σs[P(1)−O] = 5.00		Σs[P(2)−O] = 5.00		Σs[P(3)−O] = 4.97	
		3			
U(1)−F(1)	2.238(4)	U(2)−F(7)	2.190(5)		
U(1)−F(3)	2.241(5)	U(2)−F(8)	2.233(5)		
U(1)−F(5)	2.268(5)	U(2)−F(10)	2.247(4)		
U(1)−F(2)	2.273(4)	U(2)−O(2)#2	2.292(5)		
U(1)−O(8)	2.294(6)	U(2)−F(9)	2.303(4)		
U(1)−F(4)	2.356(4)	U(2)−O(1)	2.385(5)		
U(1)−O(6)	2.369(5)	U(2)−F(6)[i]	2.392(4)		
U(1)−F(4)[h]	2.392(4)	U(2)−F(6)	2.403(4)		
Σs[U(1)−O(F)] = 4.14		Σs[U(2)−O(F)] = 4.15			
P(1)−O(3)	1.489(6)	P(2)−O(5)	1.512(6)		
P(1)−O(2)	1.521(5)	P(2)−O(8)	1.518(6)		
P(1)−O(1)	1.540(5)	P(2)−O(6)[h]	1.528(5)		
P(1)−O(4)	1.579(6)	P(2)−O(7)	1.568(6)		
Σs[P(1)−O] = 5.04		Σs[P(2)−O] = 5.04			
		4			
U(1)−F(6)	2.150(4)	P(1)−O(4)	1.489(6)		
U(1)−F(7)	2.241(5)	P(1)−O(2)	1.513(6)		
U(1)−F(2)	2.272(4)	P(1)−O(3)	1.556(6)		
U(1)−F(4)	2.274(4)	P(1)−O(1)	1.574(6)		
U(1)−F(5)	2.318(5)	Σs[P(1)−O] = 5.04			
U(1)−F(1)	2.320(4)				
U(1)−F(3)	2.334(4)				
U(1)−F(1)[j]	2.482(4)				
Σs[U(1)−O(F)] = 4.04					

[a] $-x+4, -y+2, -z-1$. [b] $-x+3, -y+2, -z-1$. [c] $x-1, y, z$. [d] $-x+4, -y+1, -z-1$. [e] $-x+3, -y+1, -z-1$. [f] $-x+1, -y+1, -z+3$. [g] $-x+1, -y+1, -z+2$. [h] $-x, -y+2, -z$. [i] $-x, -y+2, -z-1$. [j] $-x+1, -y+1, -z+1$.

$_\infty[U_2F_2(PO_4)_4(HPO_4)_2]$ chain **A** along the *a* axis (Figure 3). The $[UF_2O_4]_2O_2$ dimers are each attached by six phosphate tetrahedra (four PO_4 and two HPO_4) to form the dimer motifs IIa; however, they do not self-link like motifs I but rather connect **A** chains into $2D_\infty[U_4F_6(PO_4)_4(HPO_4)_2]$ layers (Figure 4a). In such a layer, one can also find dimer motifs I and IIa that are alternately connected via edge-shared $P(3)O_4$ to form another infinite $_\infty[U_4F_6(PO_4)_6(HPO_4)_2]$ chain, **B**, along the *b* axis. Chains **A** and **B** disclose two connection modes: dimers in **A** parallel to the chain and dimers in **B** perpendicular to the chain. It is also noted that if the dimers were to be replaced by monomers, the connection skeleton of chain **B** would become the same as that of the $_\infty[UPO_4]$ chains in $CaU(PO_4)_2$.[29]

The one-dimensional (1D) chain structure of **2** contains exactly the same $[UF_2O_4]_2O_2$ dimer as in **1**, but here it is attached by two PO_4 and four HPO_4 tetrahedra to generate the dimer motif IIb. In contrast to motif IIa, dimer motifs IIb can self-link via all their PO_4 and HPO_4 tetrahedra to form the infinite $_\infty[U_2F_4(PO_4)(HPO_4)_2]$ chain **C** along the *c* axis. Chain **C** exhibits a similar connectivity to chain **B**, in that adjacent dimer motifs are oriented at nearly a right angle to each other (∼72° for **C** and ∼76° for **B**).

Compounds **3** and **4** both adopt cluster structures that consist of dimers ($[UF_4O_2]_2F_2$ and U_2F_{14}, respectively) formed from

(29) Dusausoy, Y.; Ghermani, N. E.; Podor, R.; Cuney, M. *Eur. J. Mineral.* **1996**, *8*, 667.

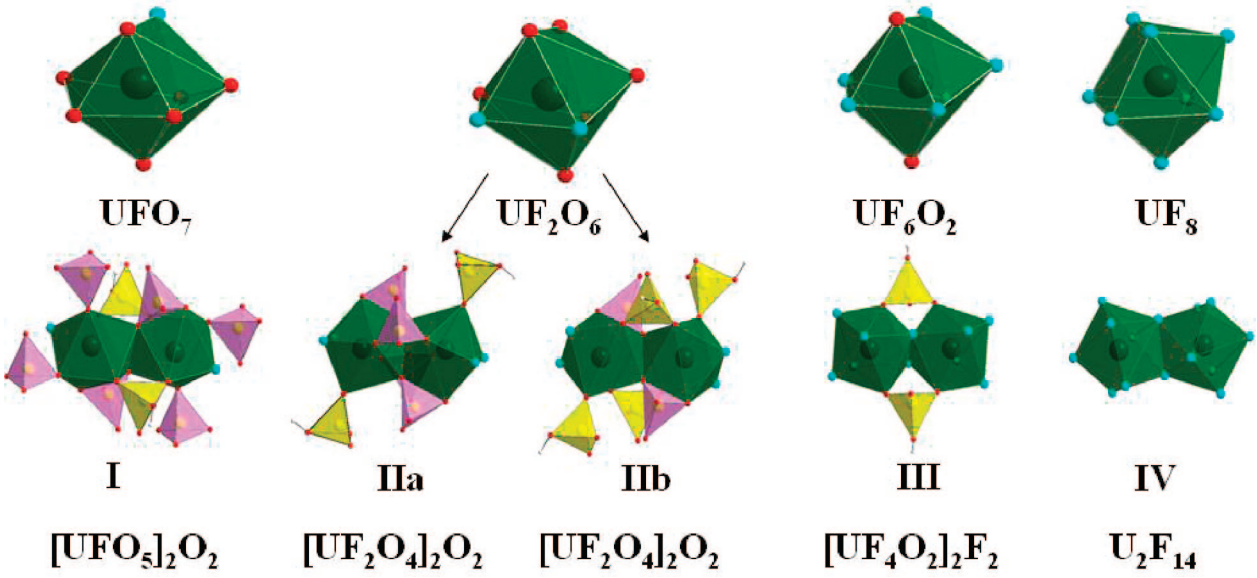

Figure 2. Polyhedral representations of the uranium BTP monomers (in green) and various dimer motifs (with PO_4 tetrahedra in pink and HPO_4 in yellow) in the structures of **1**–**4**. Phosphate oxygen ligands are shown in red and fluoride ions in cyan.

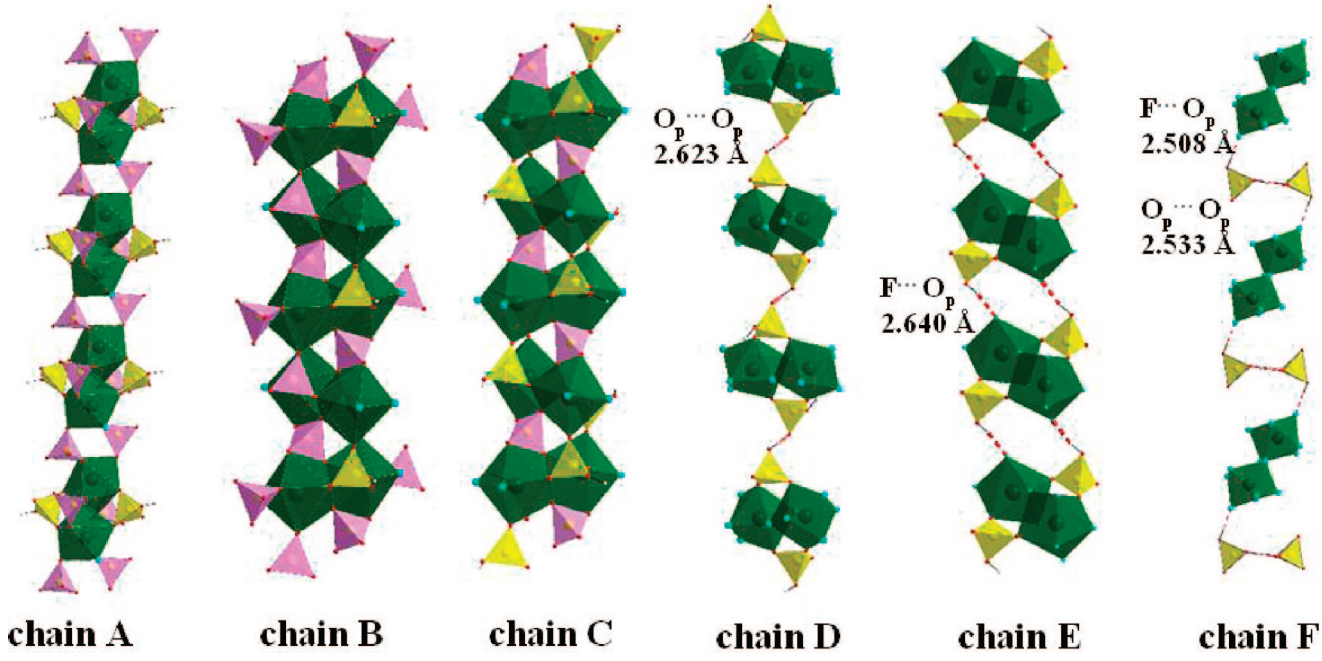

Figure 3. Linear connectivities of various dimer motifs in the structures of **1**–**4**. Dimer motifs I in chain **A**, IIa in chain **B**, and IIb in chain **C** are joined through covalent U−O−P bonds, while dimer motifs III in chains **D** and **E** are connected via hydrogen bonds. Dimer motifs IV are linked through hydrogen-bonded $(H_2PO_4)_2^{2-}$ couplets to form the supra-polyanion chain **F**.

monomers (UF_6O_2 and UF_8, respectively) that share a common F−F edge (2.545–2.574 Å). In the structure of **3**, each $[UF_4O_2]_2F_2$ dimer is attached by only two HPO_4 tetrahedra, forming highly charged, isolated clusters of $[U_2F_{10}(HPO_4)_2]^{6-}$ (dimer motif III). Compound **4** contains isolated U_2F_{14} dimers (designated as dimer motif IV) and isolated $H_2PO_4^-$ groups. It is interesting to note that the negatively charged H_2PO_4 tetrahedra are not bonded to the positively charged U^{4+} ions at all; instead, they link to each other via strong hydrogen bonds (O···O distance 2.533 Å) to form $(H_2PO_4)_2^{2-}$ couplets (Figure 3), making the structure of **4** extremely unique in the uranium phosphate system. As a consequence, two kinds of anionic clusters, $[U_2F_{14}]^{6-}$ and $(H_2PO_4)_2^{2-}$, each of which is surrounded by eight H_2dach^{2+} template cations, coexist in **4** (Figure 4f). Such a dual-anionic-cluster structure is unprecedented in metal phosphate systems.

Various Dimer Motifs and Organic Template−Solvent Effects. The U^{4+} dimer motifs I−IV are all unique, and the dimer composition can be assigned to the general formula $U_2F_mO_{14-m}$ (m = 2, 4, 10, 14), in which the value of m is related to the degree of fluorination of the central U^{4+} ions. It is interesting to note that all of these U^{4+} dimer motifs were prepared from a U^{6+} source using the same F^- and H_3PO_4 concentrations. In the literature, isolated dimers of tetravalent uranium are rather rare, since the U−O/F polyhedra show a strong disposition to polymerization; UFO-

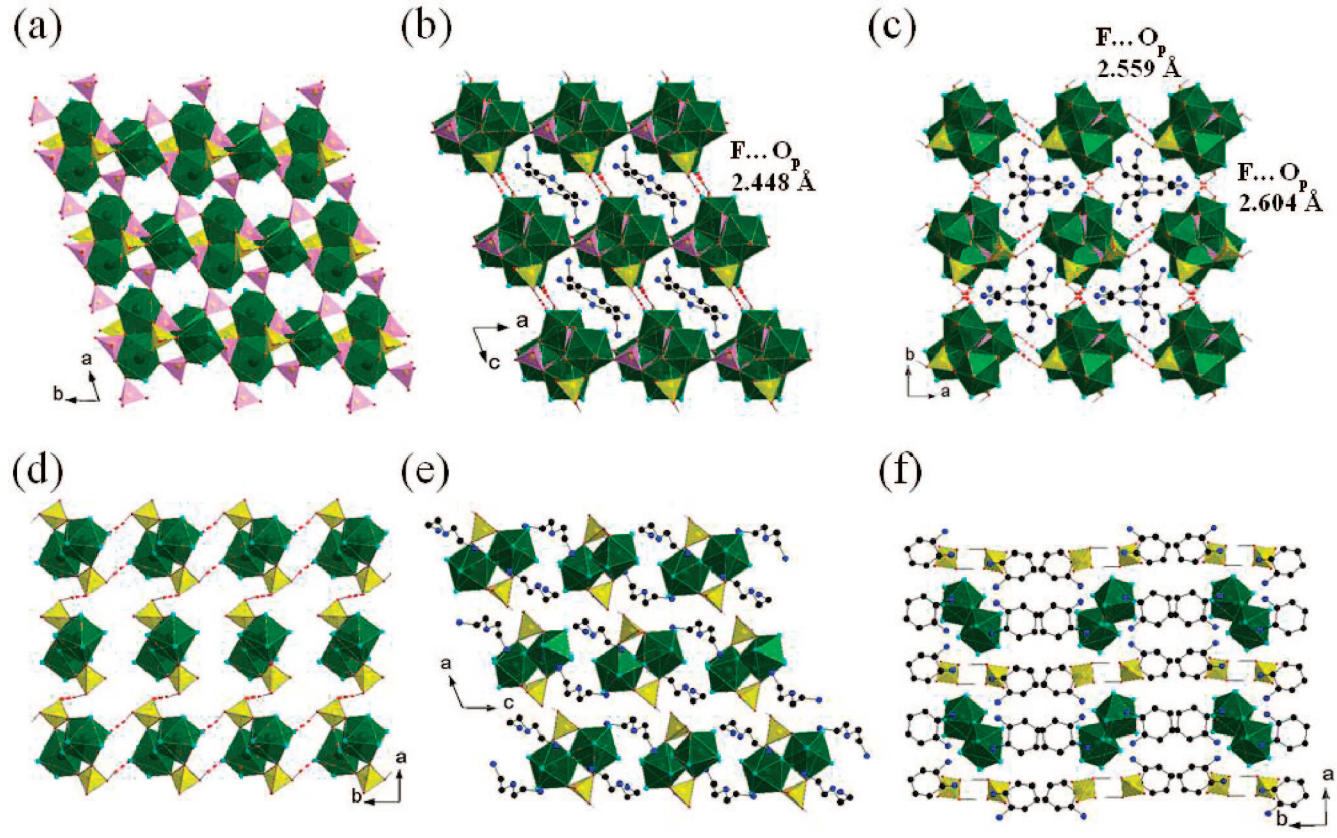

Figure 4. Structures of **1**−**4**. (a) Section of $_\infty[U_4F_6(PO_4)_4(HPO_4)_2]$ layers of **1**, formed from dimer motifs I and IIa. (b) Hydrogen-bonded 3D network of **1**, in which adjacent layers are connected via F···H−O_p bonds. (c) Hydrogen-bonded 3D network of the chain structure of **2**. (d) Section of hydrogen-bonded layers formed from chains D and E via both F···H−O_p and O_p···H−O_p hydrogen bonds. (e) Arrangement of cationic templates and anionic motifs III in **3**. (f) Two kinds of anionic clusters, $[U_2F_{14}]^{6-}$ and $(H_2PO_4)_2^{2-}$, in **4**, each of which is surrounded by eight H_2dach^{2+} template cations.

5,[12] which contains $[U_2F_{13}]^{5-}$ dimers consisting of two face-sharing UF_8 monomers, was the only example we found. In our synthesis, all of the reactions were conducted using a U^{6+} concentration that was relatively low compared with the concentrations of the other reactants. These conditions favored the creation of dispersed uranium cores that formed only dimeric units. Furthermore, the organic solvent was one of the important factors leading to the formation of these U^{4+} dimers. We noticed that U^{4+} phases could emerge only when organic solvents were employed and that the extent of reduction was pH-dependent (the reduction potential for the reduction of U^{6+} to U^{4+} is positive in acidic solution and negative in basic solution). In the preparations of **1** and **2**, we found U^{6+} dimers but no U^{4+} dimers in the products when the pH of the reaction mixtures was raised by increasing the concentration of the amine templates (see Figure S8 in the Supporting Information). In addition to being a structure-directing reagent, the amine template can influence the reaction by playing the role of a pH-adjustment chemical.[30,31] Accordingly, we found that the use of other types of amine templates having different basicities could not yield U^{4+} products from U^{6+} reactants. In addition, the reduction of U^{6+} to U^{4+} was always accompanied by fluorination, likely as a result of the large excess of HF reactant in the system. Under the synergistic interaction between the solvent and the amine template, the number of phosphate groups on the U^{4+} centers progressively decreased from 8 to zero (and the fluorination thus increased to the full extent) in going from dimer motif I to dimer motif IV.

Hydrogen-Bonding Networks. The dimensionalities of structures **1**−**4** can all be promoted by the two types of hydrogen bonds, F···H−O_p and O_p···H−O_p, between dimer motifs and hydrogen phosphate groups. It is the strong F···H−O_p bonds (2.448 Å) formed between dimer motifs I and IIa that enable the $_\infty[U_4F_6(PO_4)_4(HPO_4)_2]$ layers in **1** to become a three-dimensional (3D) hydrogen-bonded network (Figure 4b). Similarly, the strong F···H−O_p bonds (2.559 and 2.604 Å) between dimer motifs IIB can interlink the infinite chains **C** in **2** into a 3D hydrogen-bonded network as well. In contrast to **1** and **2**, the F···H−O_p and O_p···H−O_p types of hydrogen bonding both exist in **3** and **4**. Dimer motifs III are located on two crystallographic sites. Those on U(1) sites can act as hydrogen-bond donors and connect with those on U(2) sites via O_p···H−O_p bonds (2.623 Å), forming infinite hydrogen-bonded chains **D** along the *a* axis (Figure 3). In addition, dimer motifs III on the U(2) sites can connect with each other via F···H−O_p bonds (2.640 Å) to form infinite chains **E** along the *b* axis, generating a 2D hydrogen-bonded network for **3** (Figure 3). In **4**, the O_p···H−O_p bonds (2.533 Å) are located within the $(H_2PO_4)_2^{2-}$ couplets (as mentioned above), whereas the F···H−O_p bonds (2.508 Å) are found between the dimer motifs IV and the $(H_2PO_4)_2^{2-}$ couplets. Therefore, we

(30) Almond, P. M.; Deakin, L.; Mar, A.; Albrecht-Schmitt, T. E. *Inorg. Chem.* **2001**, *40*, 886.
(31) Cahill, C. L.; Burns, P. C. *Inorg. Chem.* **2001**, *40*, 1347.

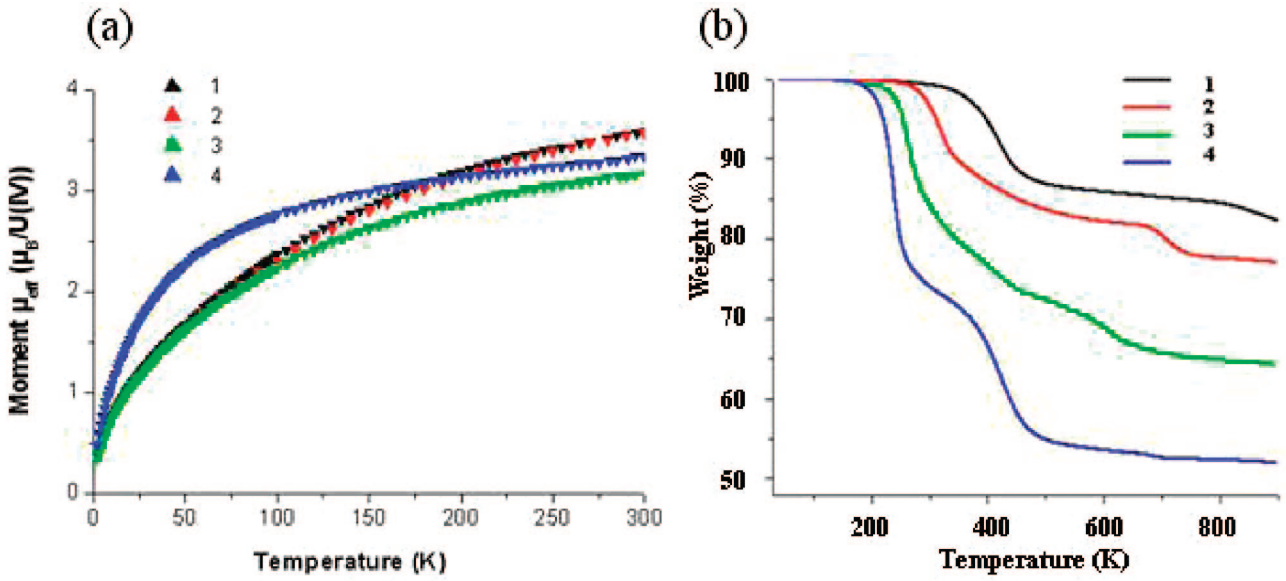

Figure 5. Plots of magnetic susceptibility (μ_{eff}) versus temperature (left) and TGA curves (right) for compounds **1**–**4**.

observe the unusual supra-polyanion chains **F** constructed from alternating $[U_2F_{14}]^{6-}$ and $(H_2PO_4)_2^{2-}$ anionic clusters. The smallest interdimer distance within the supra-polyanion chains **F** in **4** is nearly twice that within the covalent chains **A**, **B**, and **C** in **1** and **2**.

Magnetic Properties. All four compounds are paramagnetic at room temperature; their temperature-dependent μ_{eff} curves are shown in Figure 5. The effective magnetic moments at 300 K, 3.59 and 3.57 μ_B per U^{4+} center for **1** and **2**, respectively, are in good agreement with the magnetic moment of U^{4+} ion, 3.58 μ_B, expected on the basis of Russell−Saunders coupling ($g_J = {}^4/_5$ and $J = 4$) for a $^3H_4$ ground state. The effective magnetic moments of 3.35 and 3.17 μ_B per U^{4+} ion for **3** and **4**, respectively, are somewhat lower but still in the range of 3–4 μ_B per U^{4+} ion that has previously been observed in a number of reported U^{4+} compounds.[32–35] The difference in the measured room-temperature moments may be explained by magnetic anisotropy of the U^{4+} ions.[32] Fits of the magnetic susceptibilities of **1**, **2**, and **3** above 200 K and **4** above 50 K resulted in large negative Weiss constants (θ), indicating the existence of significant antiferromagnetism. Nonetheless, all four structures show a common feature: the trend of the susceptibility data below 16 K revealed a temperature-independent value of ~0.014 emu, indicating the nonmagnetic ground state of the U^{4+} ion. At ambient temperature, all four compounds displayed distinct diamagnetism after sufficient oxidation.

Thermal and Oxidizing Properties. All of the TGA curves (Figure 5) showed unresolved weight losses for the decomposition of amine templates, dehydration of hydrogen phosphates, and defluorination. The total observed weight losses (18.0, 23.0, 35.7, and 48.0%) were in good agreement with the values (18.60, 24.54, 35.65, and 48.28%) calculated on the basis of the removal of one dien, half a H_2O, and three HF from **1**; one tren, one H_2O, three HF, and half a F_2 from **2**; two dien, one H_2O, six HF, and one F_2 from **3**; and 2dach, one H_2O, four HF, and half a F_2 from **4**. These TGA curves revealed that **1** might be sustained up to ~300 °C, **2** to ~250 °C, **3** to ~200 °C, and **4** to ~180 °C. The steadily decreasing thermal stability is likely related to the dimensionalities of the inorganic lattices and their hydrogen-bonded networks.

It is worth mentioning that the chemical stability of these four U^{4+} compounds with respect to oxidization is also dimensionality-dependent. The results from oxidizing experiments under ambient conditions combined with magnetic studies indicated that the higher-dimensional structures of **1** and **2** were more stable than UO_2, since they took a longer time to oxidize into U^{6+}. Accordingly, the trend in the resistance to oxidation is **1** > **2** > UO_2 > **3** > **4**, i.e., the resistance decreases in going from the 2D layered structure of **1** to the zero-dimensional clustered structures of **4**. The results also imply that the U^{4+} ions are more stable in the phosphate matrixes with the smaller extent of fluorination.

Conclusion

This work demonstrates for the first time the successful synthesis of organically templated uranium(IV) phosphates. In this study, we prepared four new compounds having unique zero- to two-dimensional structures built up from four different types of discrete $U_2F_mO_{14-m}$ dimers enclosed by various numbers of phosphate groups. The organic template−solvent system is effective in facilitating both the reduction of uranium from the more-stable 6+ state to the less-stable 4+ state and the formation of dimer motifs. The linkage between phosphate and uranium can be covalent (as in **1**, **2**, and **3**) as well as solely hydrogen-bonded (as in **4**). This is in contrast to the water system, in which H_3PO_4 only controls the pH of the reaction mixture and does not cause the

(32) Francis, R. J.; Halasyamani, P. S.; O'Hare, D. *Chem. Mater.* **1998**, *10*, 3131.
(33) Allen, S.; Barlow, S.; Halasyamani, P. S.; Mosselmans, J. F. W.; O'Hare, D.; Walker, S. M.; Walton, R. I. *Inorg. Chem.* **2000**, *39*, 3791.
(34) Almond, P. M.; Deakin, L.; Porter, M. J.; Mar, A.; Albrecht-Schmitt, T. E. *Chem. Mater.* **2000**, *12*, 3208.
(35) Wang, C. M.; Liao, C. H.; Chen, P. L.; Lii, K. H. *Inorg. Chem.* **2006**, *45*, 1436.

formation of U−O−P bonds. We discovered that using an extremely low concentration of U^{6+} reactant played an indispensable role in promoting the formation of uranium dimers and that the synergistic interaction between the solvent and the amine template enabled the reduction of U^{6+} to U^{4+} and generated four types of U^{4+} dimer-structured topologies that are rarely observed in phosphates. Our investigation indicated that the number of phosphate groups in individual dimer motifs could be adjusted via the choice of different organic template−solvent systems, wherein uranium fluorination was autogenously controlled. Compounds **1**−**4** represent a unique series of dimer-structured materials and fill the lacuna in low-dimensional U^{4+} phosphates. The U^{4+} centers of **1** and **2**, which are embedded in a greater number of phosphate groups, appear to have greater resistance against oxidation. We expect the organic template−solvent system to be useful in preparing many more less-mobile tetravalent uranium phosphates with 3D microporous structures. Further investigation of the organic template−solvent system in the synthesis of additional uranium(IV) phosphates is in progress.

Acknowledgment. We are grateful to the National Science Council of Taiwan for support of this work (96-2628-M-007-015). S.-L.W. and K.-H.L. would also like to dedicate this paper to Professor Chan-Cheng Su on the occasion of his retirement from National Taiwan Normal University.

Supporting Information Available: X-ray crystallographic information files for **1**−**4** (CIF). Tables of ICP−AES, EA, and fluorine analysis results, ORTEP drawings, and powder XRD patterns for **1**−**4** (PDF). This material is available free of charge via the Internet at http://pubs.acs.org.

CM7027959